Check for updates

Article

INTERNATIONAL JOURNAL OF DAMAGE MECHANICS

International Journal of Damage Mechanics
2023, Vol. 32(6) 811–832
© The Author(s) 2023

Article reuse guidelines:
sagepub.com/journals-permissions
DOI: 10.1177/10567895231160810
journals.sagepub.com/home/ijd


A stress-state-dependent damage criterion for metals with plastic anisotropy

Michael Brünig, Sanjeev Koirala and Steffen Gerke

Abstract

The paper discusses the effect of stress state and of loading direction on the onset and evolution of damage in anisotropic ductile metals. A series of experiments with uniaxially and biaxially loaded specimens covering a wide range of stress states and different loading directions is used in combination with corresponding numerical simulations to develop damage criteria. The underlying continuum damage model is based on kinematic definition of damage tensors. The strain rate tensor is additively decomposed into elastic, plastic and damage parts. The anisotropic plastic behavior of the investigated aluminum alloy sheets is governed by the Hoffman yield condition taking into account the strength-differential effect revealed by uniaxial tension and compression tests. Based on this yield criterion generalized anisotropic stress invariants as well as the generalized stress triaxiality and the generalized Lode parameter are defined characterizing the stress state in the anisotropic ductile metal. A damage criterion formulated in terms of these anisotropic stress invariants is proposed and damage mode parameters allow adequate consideration and combination of different damage processes on the micro-level. At the onset of damage the anisotropic stress parameters are determined. With these experimental-numerical data the damage mode parameters are identified depending on stress state and loading direction.

Keywords

Biaxial experiments, numerical simulations, Hoffman yield criterion, damage criterion, anisotropic sheet metals

Introduction

Engineering materials have to fulfill several demands to reduce energy consumption, to enforce safety requirements, to increase lifetime and to improve cost efficiency. For example, to develop an efficient design of structural components in the automotive industries an important aspect is the evaluation of the forming severity. In this context, necking can be seen as a major failure process

Institut für Mechanik und Statik, Universität der Bundeswehr München, Neubiberg, Germany

Corresponding author:
Michael Brünig, Institut für Mechanik und Statik, Universität der Bundeswehr München, Werner-Heisenberg-Weg 39, 85577 Neubiberg, Germany.
Email: michael.bruenig@unibw.de

indicating loss of load carrying capacity. Therefore, new high quality metals and alloys have been developed with optimized material properties to reduce localization of irreversible strains as well as damage and failure during loading. Since damage and fracture may cause remarkable problems accurate prediction of the performances of these ductile metals is very important. Thus, development of accurate and practically applicable material models is necessary to perform numerical simulations of complex loading processes. To validate the constitutive approach experiments covering a wide range of stress states and loading histories have to be performed.

Many experiments with various specimens have been proposed in the literature to examine inelastic deformation behavior and damage processes. In particular, results of tests with uniaxially loaded specimens with unnotched and notched geometries have been reported by Bao and Wierzbicki (2004), Bonora et al. (2005), Bai and Wierzbicki (2008), Brünig et al. (2008), Gao et al. (2010), Li et al. (2011), and Dunand and Mohr (2011) investigating the effect of the stress state on damage and fracture mechanisms. Special geometries for uniaxially loaded specimens have been developed by Bao and Wierzbicki (2004), Brünig et al. (2008), Gao et al. (2010), Driemeier et al. (2010), Li et al. (2011), Roth and Mohr (2016), Lou et al. (2017), and Liu et al. (2019) to analyze the deformation and failure behavior under shear dominated stress states. Combined shear-tension tests with aluminum tubes have been proposed by Scales et al. (2019). To cover a wide range of stress states experiments with biaxially loaded cruciform specimens have been presented by Demmerle and Boehler (1993), Lin and Ding (1995), Müller and Pöhland (1996), Green et al. (2004), Kuwabara (2007), Kulawinski et al. (2011), and Song et al. (2017). For studies of stress-state-dependent damage and fracture mechanisms in ductile metals Brünig et al. (2015a, 2015b) and Gerke et al. (2017) proposed new geometies for biaxially loaded specimens. These new specimens have been extensively used to analyze the influence of non-proportional load paths (Brünig et al., 2019; Gerke et al., 2020) or the effect of loading direction in anisotropic metals (Brünig et al., 2021, 2022) on damage and failure behavior.

In automotive and aeronautical industries metals can be deformed by various manufacturing process such as rolling, extrusion or deep drawing to produce thin sheets. These forming operations often lead to anisotropies due to internal changes in the crystallographic structure. To simulate the mechanical behavior of these thin sheets in an accurate manner the deformation-induced anisotropies have to be taken into account in the constitutive model. For example, Hill (1948) proposed an anisotropic generalization of the von Mises criterion with a quadratic function of stresses. For plane stress applications identification of material parameters is also based on r-values which are defined assuming isochoric plastic deformations and are computed using measured plastic strain increments during loading in different directions with respect to the rolling direction. Badreddine et al. (2015) and Badreddine and Saanouni (2017) used this yield condition with kinematic hardening in their continuum damage model. Barlat et al. (2005), Ha et al. (2018), and Hu et al. (2021) presented anisotropic yield conditions with non-quadratic functions where identification of material parameters is based on results of uniaxial and equi-biaxial tension tests. Alternatively, Stoughton and Yoon (2009) discussed a quadratic yield criterion combined with four hardening curves taken from uniaxial tension tests along rolling, diagonal and transverse directions as well as from equi-biaxial tests. In addition, based on results of cruciform hole expansion tests Tsutamori et al. (2020) developed a spline yield condition showing better accuracy than conventional anisotropic yield functions proposed by Hill (1948) and Barlat et al. (2005). Furthermore, many metals show different yield behavior under tension and compression loading (Spitzig et al., 1975, 1976; Spitzig and Richmond, 1984). This strength-differential (SD) effect is also examined in the present paper and the anisotropic plastic behavior is proposed to be modeled by the Hoffman yield criterion (Hoffman, 1967) which was developed to investigate failure in composite structures.

Furthermore, in engineering applications accurate information on the influence of micro-defects on stress states in multi-axially loaded structures is needed. Thus, modeling of damage in materials has received remarkable attention and different damage models have been proposed based on experiments and numerical simulations, see Lemaitre (1985), Chow and Wang (1987), Chaboche (1988), Brünig (2003), Abu Al-Rub and Voyiadjis (2003), and Badreddine and Saanouni (2017), among others. In these approaches internal deterioration of material properties is taken into account and, therefore, they can be seen as a tool between elastic plastic continuum and fracture mechanics. Critical values of damage variables can be taken to predict onset of macro-cracking.

In the present paper, results of experiments with the X0- and the H-specimen performed by Brünig et al. (2021, 2022) are used to develop the anisotropic plastic model and the damage condition which has been applied to the aluminum alloy EN AW-2017A (EN AW-AlCu4MgSi). The experiments clearly showed that the stress state as well as the loading direction influenced the damage mechanisms on the micro-level and, therefore, both dependencies are here taken into account. The analysis is based on a continuum model where the anisotropic plastic behavior including the SD effect is governed by the Hoffman yield criterion. Corresponding generalized stress invariants based on this condition are formulated and the current stress state is characterized by the generalized stress triaxiality and the generalized Lode parameter. With these parameters a stress-state-dependent damage criterion for ductile metals with plastic anisotropy is proposed taking into account different damage mechanisms in a phenomenological way. Numerical simulation of a series of experiments based on the elastic-plastic model are performed to identify the onset of damage in the respective tests with uniaxially and biaxially loaded specimens cut in different directions with respect to the rolling direction. Analysis of stress states in critical parts of the specimens is used to develop stress-state- and loading-direction-dependent functions for the damage criterion.

Continuum model

Analysis of inelastic deformations and damage behavior of ductile metals is based on the continuum framework developed by Brünig (2003), Brünig et al. (2013), and Brünig (2016). Their phenomenological model considers isotropic plastic behavior and is based on experimental and numerical studies on both the micro- and the macro-level examining various mechanisms acting on these scales as well as their interaction. To enhance this continuum model for anisotropic plasticity a series of multiaxial tests has been performed by Brünig et al. (2021, 2022). These experiments reveal the influence of the loading direction on evolution of inelastic deformations and on damage and failure mechanisms.

The basic idea of the continuum damage approach is the definition of the damage strain tensor, $\mathbf{A}^{da}$, quantifying the stress-state-dependent evolution of macroscopic inelastic strains caused by formation of microscopic damage processes. In addition, the basic equations are formulated with respect to damaged and fictitious undamaged configurations, respectively. The kinematic approach is based on the introduction of metric transformation tensors and, thus avoids the explicit introduction of rotations and spin tensors. It leads to the additive decomposition of the strain rate tensor into elastic, $\dot{\mathbf{H}}^{el}$, effective plastic, $\bar{\dot{\mathbf{H}}}^{pl}$, and damage parts, $\dot{\mathbf{H}}^{da}$ as well as to the definition of logarithmic strains, see Brünig (2003) for further details.

The fictitious undamaged configurations are considered to formulate the isotropic elastic law leading to the effective Kirchhoff stress tensor

$$\bar{\mathbf{T}} = \bar{T}^{i}_{\cdot j}\,\mathbf{g}_i \otimes \mathbf{g}^j = 2G\mathbf{A}^{el} + \left(K - \frac{2}{3}G\right)\mathrm{tr}\mathbf{A}^{el}\mathbf{1} \tag{1}$$

where G and K are the constant shear and bulk modulus and $\mathbf{A}^{el}$ represents the elastic strain tensor. During rolling of ductile sheets the manufacturing process may lead to plastic anisotropy. In the present theoretical approach it is assumed that the principal axes of the stress tensor (1) coincide with the axes of plastic anisotropy. These principal axes are the x-direction of rolling (RD, 0°), the y-direction transversely in the plane of the sheet (TD, 90°) and the z-direction normal to the sheet plane. In addition, results of different uniaxial tension and compression tests have shown different yield stresses and, therefore, the strength-differential (SD) effect also revealed by Spitzig et al. (1975, 1976) and Spitzig and Richmond (1984) in different metals has to be taken into account. Thus, onset of plastic yielding of ductile metals is governed by the Hoffman yield condition (Hoffman, 1967)

$$f^{pl} = \mathbf{C} \cdot \bar{\mathbf{T}} + \sqrt{\frac{1}{2}\bar{\mathbf{T}} \cdot \mathcal{D}\,\bar{\mathbf{T}}} - c = 0 \tag{2}$$

where the strength-differential effect is characterized by the tensor of coefficients

$$\mathbf{C} = C^{i}_{.j}\,\mathbf{g}_i \otimes \mathbf{g}^j = C_{(i)}\,\mathbf{g}_i \otimes \mathbf{g}^i \tag{3}$$

with the components (in Voigt notation)

$$[C^{i}_{.j}] = [C_1 \quad C_2 \quad C_3 \quad 0 \quad 0 \quad 0]^T \tag{4}$$

Further material parameters modeling the plastic anisotropy are included in the tensor

$$\mathcal{D} = D^{i.k}_{.j.l}\,\mathbf{g}_i \otimes \mathbf{g}^j \otimes \mathbf{g}_k \otimes \mathbf{g}^l \tag{5}$$

with

$$[D^{i.k}_{.j.l}] = \begin{bmatrix} C_4 + C_5 & -C_4 & -C_5 & 0 & 0 & 0 \\ -C_4 & C_4 + C_6 & -C_6 & 0 & 0 & 0 \\ -C_5 & -C_6 & C_5 + C_6 & 0 & 0 & 0 \\ 0 & 0 & 0 & C_7 & 0 & 0 \\ 0 & 0 & 0 & 0 & C_8 & 0 \\ 0 & 0 & 0 & 0 & 0 & C_9 \end{bmatrix} \tag{6}$$

and c denotes the equivalent yield stress of the undamaged material identified by a chosen uniaxial reference test. It should be noted that the Hoffman criterion (2) can be seen as a hydrostatic-stress-dependent generalization of the anisotropic Hill condition (Hill, 1948) which has been used by Brünig et al. (2021, 2022) to analyze the anisotropic plastic behavior of the investigated aluminum alloy without considering the SD effect.

For isotropic material behavior stress invariants can be taken into account to characterize the stress state. With these invariants it is possible to define the stress triaxiality and the Lode parameter which are often used to develop stress-state-dependent functions (see, for example, Brünig et al., 2013). Badreddine et al. (2015) and Badreddine and Saanouni (2017) modeled the anisotropic plastic behavior with the Hill yield condition and used the classical isotropic definition of the stress triaxiality given by the ratio of the mean and the von Mises equivalent stress. Similarly, Hosseini et al.

(2022) studied the effect of material orientation on void growth based on the orthotropic Yld2004 yield criterion (Barlat et al., 2005) also using the classical isotropic definition of the stress triaxaility and the Lode parameter expressed in terms of the principal stresses. However, in the analysis of anisotropic materials it is important to take into account the directionality of the stress state with respect to the material orientation and, therefore, a generalized stress triaxiality and Lode parameter have to be developed. In this context, to examine ductile fracture of anisotropic metals Park et al. (2017) suggested the Lou-Huh criterion (Lou et al., 2012; Lou and Huh, 2013) and proposed an anisotropic stress triaxiality based on Hill's yield condition (Hill, 1948). Park et al. (2018) recommended an alternative definition of the stress triaxiality taking into account the Yld91 criterion (Barlat et al., 1991). However, in these anisotropic definitions only the equivalent stress is based on an anisotropic yield condition whereas the classical definition of the mean stress with the trace of the stress tensor is used. In addition, the Lode parameter is classically formulated with the principal stress values.

Since all parameters characterizing the stress state in anisotropic metals should take into account the material orientation, in the present paper, generalized invariants are introduced based on the Hoffman yield condition (2). In particular, the first Hoffman invariant is defined as

$$\bar{I}_1^H = \frac{1}{a}\mathbf{C}\cdot\bar{\mathbf{T}} \quad \text{with} \quad a = \frac{1}{3}\,\text{tr}\mathbf{C} \tag{7}$$

whereas the second and third deviatoric invariants are given by

$$\bar{J}_2^H = \frac{1}{2}\bar{\mathbf{T}}\cdot\mathcal{D}\bar{\mathbf{T}} \tag{8}$$

and

$$\bar{J}_3^H = \det(\mathcal{D}\bar{\mathbf{T}}) \tag{9}$$

Based on these Hoffman invariants the generalized Hoffman stress triaxiality

$$\bar{\eta}^H = \frac{\bar{I}_1^H}{3\sqrt{3\bar{J}_2^H}} \tag{10}$$

and the generalized Hoffman Lode parameter

$$\bar{L}^H = \frac{-3\sqrt{3}\,\bar{J}_3^H}{2\left(\bar{J}_2^H\right)^{(3/2)}} \tag{11}$$

are defined characterizing the stress state dependence of plastically anisotropic metals.

With the introduction of the generalized invariants (7) to (9) the Hoffman yield condition (2) can be rewritten in the form

$$f^{pl} = a\,\bar{I}_1^H + \sqrt{\bar{J}_2^H} - c = 0 \tag{12}$$

Spitzig and Richmond (1984) reported that during their experiments with tension and compression tests superimposed by various hydrostatic pressures only marginal plastic volume increases in ductile metals have been measured and, thus, plastic incompressibility is assumed. Therefore, the evolution of plastic strains during loading is governed by a non-associated flow rule. Based on the plastic potential function

$$g^{pl} = \sqrt{\bar{J}_2^H} \tag{13}$$

the effective plastic strain rate is given by

$$\dot{\bar{\mathbf{H}}}^{pl} = \dot{\bar{\lambda}} \frac{\partial g^{pl}}{\partial \bar{\mathbf{T}}} = \dot{\lambda} \mathcal{D} \bar{\mathbf{T}} = \dot{\gamma} \bar{\mathbf{N}} \tag{14}$$

where the non-negative scalar factors $\dot{\lambda}$ and $\dot{\gamma}$ as well as the normalized deviatoric effective stress tensor $\bar{\mathbf{N}}$

$$\dot{\lambda} = \dot{\bar{\lambda}} \frac{1}{2\sqrt{\bar{J}_2^H}}, \quad \dot{\gamma} = \dot{\lambda} \| \mathcal{D} \bar{\mathbf{T}} \| \text{ and } \bar{\mathbf{N}} = \frac{\mathcal{D} \bar{\mathbf{T}}}{\| \mathcal{D} \bar{\mathbf{T}} \|} \tag{15}$$

have been used.

Furthermore, the damaged configurations are considered to formulate equations modeling the damage behavior of ductile metals (Brünig, 2003, 2016). In particular, the Kirchhoff stress tensor

$$\begin{aligned} \mathbf{T} = {} & 2(G + \eta_2 \operatorname{tr}\mathbf{A}^{da})\mathbf{A}^{el} \\ & + \left[\left(K - \frac{2}{3} G + 2\eta_1 \operatorname{tr}\mathbf{A}^{da} \right) \operatorname{tr}\mathbf{A}^{el} + \eta_3 (\mathbf{A}^{da} \cdot \mathbf{A}^{el}) \right] \mathbf{1} \\ & + \eta_3 \operatorname{tr}\mathbf{A}^{el} \mathbf{A}^{da} + \eta_4 (\mathbf{A}^{el}\mathbf{A}^{da} + \mathbf{A}^{da}\mathbf{A}^{el}) \end{aligned} \tag{16}$$

takes into account the experimentally observed deterioration of elastic properties caused by damage mechanisms on the micro-level. Therefore, in contrast to the effective Kirchhoff stress tensor (1) defined in the undamaged configurations it depends on both the elastic and the damage strain tensors, $\mathbf{A}^{el}$ and $\mathbf{A}^{da}$. The additional constitutive parameters η_1, η_2, η_3 and η_4 quantify the deterioration effect.

It has been observed in many experiments with ductile metals that damage mechanisms on the micro-level strongly depend on the stress state: during tensile loading with high positive stress triaxialities the predominant damage processes are nucleation, growth and coalescence of microvoids, during shear and compressive loading with small positive or negative stress triaxialities the main mechanisms are formation and growth of micro-shear-cracks and for moderate positive stress triaxialities damage is a combination of these basic processes whereas no formation of damage has been detected for high negative stress triaxialities (Brünig et al., 2018). Thus, the onset and evolution of damage in plastically anisotropic metals is characterized by the damage condition

$$f^{da} = \alpha I_1^H + \beta \sqrt{J_2^H} - \sigma = 0 \tag{17}$$

where I_1^H and J_2^H are the generalized first and second deviatoric Hoffman invariants of the Kirchhoff stress tensor (16), and σ represents the equivalent damage stress. It should be noted that at the onset of damage the effective Kirchhoff stress tensor $\bar{\mathbf{T}}$ and the Kirchhoff stress tensor $\mathbf{T}$ are identical and, therefore, the respective generalized invariants, the generalized stress triaxialities and the generalized Lode parameters with respect to the undamaged and the damaged configurations also coincide (for example, $\bar{\eta}^H = \eta^H$, $\bar{L}^H = L^H$). The stress-state-dependent factors α and β are the damage mode parameters corresponding to the above mentioned damage mechanisms acting on the micro-level. The focus of the present paper is the identification of these parameters α and β and their dependence on the loading direction with respect to the rolling direction.

In addition, the damage strain rate tensor

$$\dot{\mathbf{H}}^{da} = \dot{\mu}\,\frac{\partial g^{da}}{\partial \mathbf{T}} \tag{18}$$

predicts formation of irreversible macroscopic strains caused by damage processes on the micro-scale in a phenomenological macroscopic way. In equation (18) $\dot{\mu}$ represents the equivalent damage strain rate and

$$g^{da} = \hat{\alpha} I_1^H + \hat{\beta}\,(J_2^H)^{(1/2)} + \hat{\delta}\,(J_3^H)^{(1/3)} \tag{19}$$

is the damage potential function expressed in terms of the generalized stress invariants and $\hat{\alpha}, \hat{\beta}, \hat{\delta}$ are kinematic parameters characterizing the portion of volumetric and isochoric damage strain rates corresponding to void growth and micro-shear-crack mechanisms on the micro-level.

Material and elastic-plastic parameters

The aluminum alloy EN AW-2017A (EN AW-Al Cu4MgSi) taken from 4 mm thick sheets is analyzed in detail. Uniaxial tension and compression as well as shear tests taken from the sheets in different directions with respect to the rolling direction (0°, 45°, 90°) have been performed to identify the material parameters. Figure 1(a) shows the geometry for the flat dog-bone-shaped specimens for the tension and compression tests. It is characterized by a short uniform part allowing compression tests without early occurrence of buckling. In addition, shear tests have been carried out with new specimens where the symmetric geometry is characterized by two notched parts (Figure 1(b)). Details of the geometry of the central region with notches are shown in Figure 1 (c). During the respective experiments three-dimensional displacement fields on the surfaces of the specimens have been monitored by digital image correlation (DIC) using a four-camera system with one pair on the front and one pair on the back surface of the specimen (see Brünig et al. (2022) for further details).

From the uniaxial tests, true stress–true plastic strain curves are shown in Figure 2(a). Comparison of the respective tension and compression tests shows the SD-effect with smaller initial yield stresses under compression than under tensile loading. During further compressive loading a more pronounced increase in yield stress can be seen which might be a result of 3D-effects caused by non-homogeneous inelastic deformations of the short specimen and, thus, will not be taken into account in the present analysis. The material parameters for isotropic elastic behavior are determined: Young's modulus $E = 74{,}000$ MPa and Poisson's ratio $\nu = 0.3$. The plastic behavior is characterized by the reference yield stress

$$c = c_o + R_o \epsilon^{pl} + R_\infty (1 - e^{-b\epsilon^{pl}}) \tag{20}$$

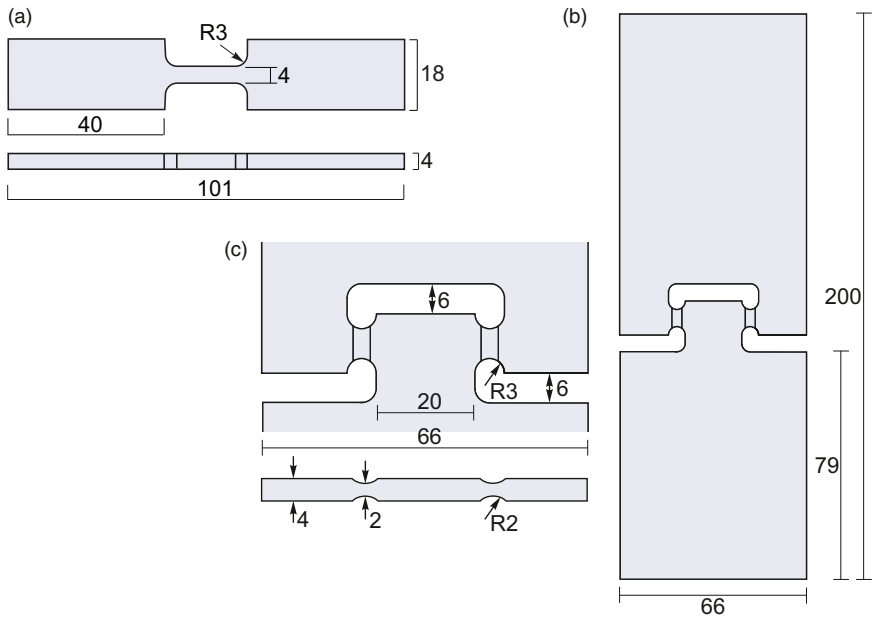

Figure 1. (a) Tension/compression specimen, (b) Shear specimen and (c) Central part of the shear specimen; all dimensions in mm.

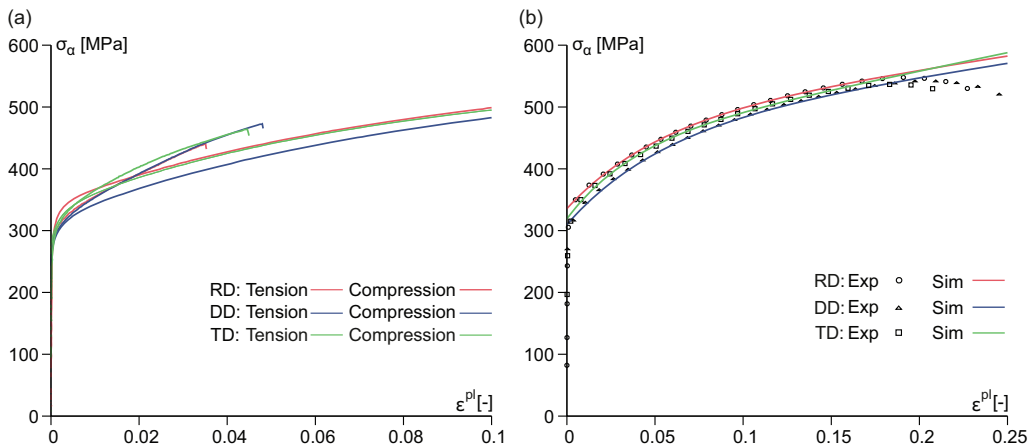

Figure 2. (a) Uniaxial true stress–uniaxial true plastic strain curves for tension and compression tests and (b) Numerical simulation of the tension tests.

of the tensile test with the specimen cut in rolling direction (RD) where c_o is the initial yield stress, R_o and R_∞ represent the hardening moduli, b means the hardening exponent and ϵ^{pl} denotes the uniaxial plastic strain in loading direction. For the investigated aluminum alloy the material parameters for the reference test are shown in Table 1. Excellent agreement of experimental curves and the numerically predicted ones based on equation (20) can be seen in Figure 2(b). It should be noted

Table 1. Plastic material parameters.

	c_o [MPa]	R_o [MPa]	R_∞ [MPa]	b
RD	333	488	142	19

RD: rolling direction.

that the final drop in stresses in the experiments is mainly caused by damage processes and cannot be simulated by this plastic law (20). It should be noted that in the present analysis only isotropic hardening is considered because in all experiments monotonic loading paths occurred whereas for reverse or cyclic loading conditions a kinematic or mixed (isotropic-kinematic) model has to be taken into account (Wei et al., 2022).

Identification of anisotropic material parameters of thin metal sheets is restricted to tests with flat specimens cut in the plane of the sheet and, therefore, plane stress conditions are taken into account where all stresses in the plane with the normal in z-direction are taken to be marginal. In particular, from the tension (T) and compression (C) tests with specimens cut in RD (x-direction) the parameter

$$C_1 = \frac{1}{2}\left(1 - \frac{\bar{T}_{Tx}}{\bar{T}_{Cx}}\right) \tag{21}$$

and from the tension and compression tests with specimens cut in TD (y-direction) the parameter

$$C_2 = \frac{1}{2}\bar{T}_{Tx}\left(\frac{1}{\bar{T}_{Ty}} - \frac{1}{\bar{T}_{Cy}}\right) \tag{22}$$

can be determined where $\bar{T}_{Tx} = c_o$ (20) represents the initial yield stress of the reference experiment (tensile test in RD).

Further anisotropy parameters can be identified by an alternative indirect method based on the ratios of measured plastic strain increments in uniaxially loaded specimens cut in RD and TD as well in the diagonal direction (DD, 45°). Taking into account plastic incompressibility this leads to the Lankford coefficients

$$r_\theta = \frac{-\dot{\bar{H}}^{pl}_{\theta+90^\circ}}{\dot{\bar{H}}^{pl}_{x} + \dot{\bar{H}}^{pl}_{y}} \tag{23}$$

where θ is the angle with respect to the rolling direction, see Brünig et al. (2021) for further details.

Based on the results of the tension test with the specimen cut in RD the parameter. The Lankford coefficients for different directions are shown in Table 2

$$C_5 = \frac{1}{2(1 + r_{0^\circ})}\left(1 + \frac{\bar{T}_{Tx}}{\bar{T}_{Cx}}\right)^2 \tag{24}$$

and the parameter

$$C_4 = r_{0^\circ}\, C_5 = \frac{1}{2}\left(1 + \frac{\bar{T}_{Tx}}{\bar{T}_{Cx}}\right)^2 - C_5 \tag{25}$$

Table 2. Lankford coefficients.

r_{0°	r_{45°	r_{90°
0.597	0.783	0.695

are computed. The tension test with the specimen cut in TD leads to the parameter

$$C_6 = \frac{C_4}{r_{90^\circ}} \tag{26}$$

which can be seen as a plastic strain-based definition. Alternatively, using the reference test in RD and the tension test in y-direction this parameter is given by

$$C_6 = \frac{1}{2}\bar{T}_{Tx}^2\left(\frac{1}{\bar{T}_{Ty}} + \frac{1}{\bar{T}_{Cy}}\right)^2 - C_4 \tag{27}$$

leading to a stress-based definition of C_6. Brünig et al. (2021) have shown that results based on equation (26) lead to deviations with experimentally determined yield stresses whereas analysis based on equation (27) leads to differences in r-values. They showed that numerical calculations based on the mean value of both equations leads to good agreement of both the numerically predicted yield stresses and the r-values with test results for specimens cut in different directions. In addition, measured plastic strain increments from tension tests with specimens cut in DD lead to the parameter

$$C_7 = \left(r_{45^\circ} + \frac{1}{2}\right)(C_5 + C_6) \tag{28}$$

which is the plastic strain-based definition of the parameter C_7. Alternatively, this parameter can be identified using the yield stress of the shear test (S). Then, in the case of shear stress only this parameter is identified by the stress-based definition

$$C_7 = \left(\frac{\bar{T}_{Tx}}{\bar{T}_{Sxy}}\right)^2 \tag{29}$$

If in the critical region additional normal stresses $\bar{T}_x$ are numerically predicted the parameter C_7 is given by

$$C_7 = \frac{1}{\bar{T}_{Sxy}^2}\left[(\bar{T}_{Tx} - C_1\,\bar{T}_x)^2 - \frac{1}{2}(C_4 + C_5)\bar{T}_x^2\right] \tag{30}$$

In the present analysis the parameter C_7 is taken to be the mean value of the results of equations (28) and (30). For the investigated aluminum alloy these parameters are listed in Table 3.

Table 3. Anisotropy parameters.

C_1	C_2	C_3	C_4	C_5	C_6	C_7	C_8	C_9
−0.0424	−0.0102	0.0	0.8123	1.3607	1.3103	3.7580	3.0	3.0

Experimental and numerical aspects

The tension, compression and shear tests with uniaxially loaded specimens discussed above have been used to identify the elastic-plastic parameters for the anisotropic ductile metal which serve as input parameters in the numerical simulations. On the other hand, series of experiments with biaxially loaded specimens have been performed to investigate the stress-state-dependent damage behavior as well as to study the effect of the loading direction on damage and failure mechanisms in anisotropic metals. In particular, the X0- and the H-specimen have been extensively tested by Brünig et al. (2021, 2022) considering different load ratios leading to a wide range of stress states in notched parts where damage occurred. They also studied the influence of the orientation of the specimens with respect to the principal axes of anisotropy during loading and concluded that in both specimens loading in RD and TD leads to more and larger micro-voids whereas during loading in DD more pronounced micro-shear-cracks are formed. The experimental results reported in Brünig et al. (2021, 2022) are used in the present paper to develop the stress-state- and loading-direction-dependent damage criterion (17).

The biaxial experiments were carried out with the biaxial test machine type LFM-BIAX 20 kN (produced by Walter & Bai, Switzerland) containing four electro-mechanically, individually driven actuators, see Figure 3(a). The specimens were clamped in the four heads of the actuators and during the tests they were biaxially strained with proportional load paths. During the experiments three-dimensional displacement fields in notched regions of the specimen were monitored by DIC using stereo setting with eight 6.0 Mpx cameras (Figure 3(b)). More details on the experimental equipment are given in Brünig et al. (2021, 2022).

Details of the geometries of the X0- and the H-specimen are shown in Figure 4. The outer dimensions are 240 mm in both directions (Figure 4(c)) and in their central parts four notches in thickness direction are milled (Figure 4(d) and (h)) leading to a reduction in thickness up to 2 mm (Figure 4(f) and (i)). The respective notch radii are 2 mm in thickness and 3 mm in plane direction (Figure 4(e) and (j)). The specimens are simultaneously loaded in two perpendicular directions by the forces F_1 and F_2 (Figure 4(b) and (k)) leading to high tensile or shear stresses in the X0-specimen whereas in the H-specimen combinations of shear stresses with superimposed tensile or compressive stresses can be reached. During the experiments, displacements of the red points shown in Figure 4 (b) and (k) are recorded by DIC which are used to compute the relative displacements $\Delta u_{ref.1} = u_{1.1} - u_{1.2}$ in direction 1 and $\Delta u_{ref.2} = u_{2.1} - u_{2.2}$ in direction 2 shown in the load–displacement curves.

Furthermore, numerical analysis of the respective experiments with the biaxially loaded specimens has been performed to predict the stress states at the onset of damage. The corresponding numerical simulations are based on the finite element program ANSYS enhanced by a user-defined subroutine taking into account the elastic-plastic material model discussed above. The numerical procedure is based on the plastic predictor–elastic corrector method leading to fast convergence of the numerical results and numerical stability of the algorithm, see Brünig (1999). Using symmetry boundary conditions a quarter of the X0-specimen is divided into 18,645 eight-node elements of type SOLID185 (Figure 5(a)) whereas the H-specimen is discretized by 20,802 elements, see Figure 5 (b). Remarkable refinements of the finite element meshes are used in the respective central notched

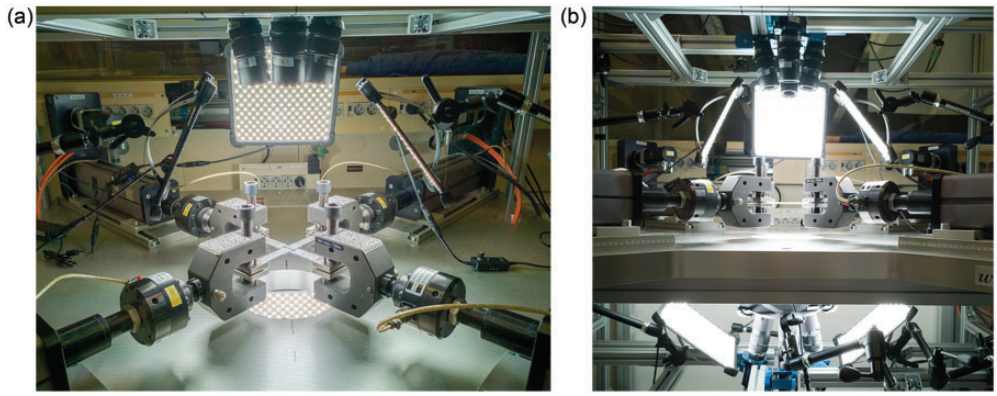

Figure 3. (a) Biaxial test machine and (b) lighting system and camera equipment (Brünig et al., 2021, 2022).

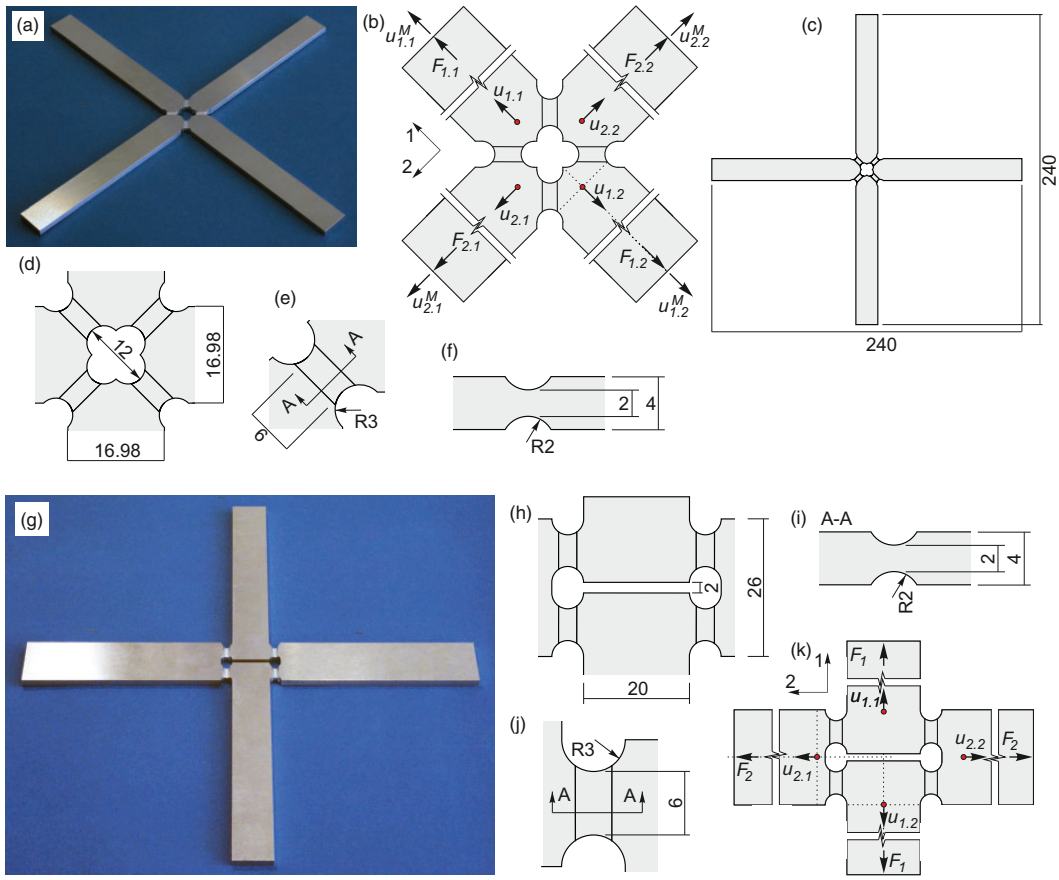

Figure 4. Details of the geometry of the X0- ((a)–(f)) and the H-specimen ((g)–(k)); all dimensions in mm (Brünig et al., 2021, 2022).

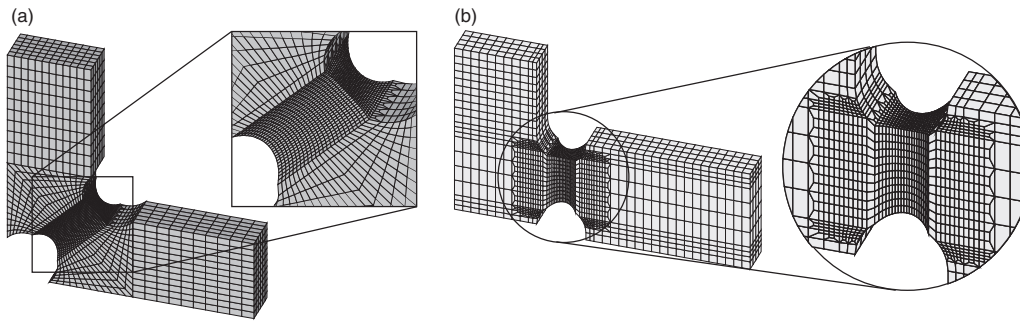

Figure 5. Finite element meshes of (a) the X0-specimen (Brünig et al., 2021) and (b) the H-specimen (Brünig et al., 2022).

parts where high stress gradients are expected to occur. The displacements act on the nodes at the end faces and out-of-plane deflections are suppressed by zero displacements in the symmetry planes.

Experimental and numerical results

Results of experiments with uni- and biaxially loaded specimens and corresponding numerical simulations are used to develop a damage criterion for the investigated anisotropic aluminum alloy.

Brünig et al. (2008) proposed that based on elastic-plastic numerical simulations damage is assumed to be initiated when discrepancies between numerically predicted and experimentally obtained load-displacement curves occur. They reported that in their experiments with uniaxially loaded specimens it was easy to identify this critical point. Therefore, this identification method is also used in the present analysis with the uniaxially loaded tension and shear specimens as well as with the biaxially loaded X0- and H-specimens. At this stage of loading various stress quantities are determined in the region of the maximum equivalent plastic strain where onset of damage is expected to occur. The parameters are used to develop the functions of the stress-state- and loading-direction-dependent parameters α and β in the damage condition (17). In particular, based on the Hoffman criterion the generalized stress invariants, $\bar{I}_1^H$ (7), $\bar{J}_2^H$ (8) and $\bar{J}_3^H$ (9), the generalized stress triaxiality $\bar{\eta}^H$ (10) and the generalized Lode parameter $\bar{L}^H$ (11) are listed in Table 4 for all available experiments for loading in RD, DD and TD, respectively.

Following Bao and Wierzbicki (2004) and Brünig et al. (2008) it seems to be convenient to distinguish three regions of stress triaxialities and to develop in these regions an analytical expression for the stress-state-dependent damage parameters α and β. In particular, for high stress triaxialities damage is due to nucleation, growth and coalescence of micro-voids caused by predominant hydrostatic stresses. For nearly zero or negative stress triaxialities the main damage mechanism is formation and growth of micro-shear-cracks caused by predominant shear or deviatoric stresses. And for moderate positive stress triaxialities damage is caused by both mechanisms simultaneously whereas no damage was observed in experiments with high negative stress triaxialities (Brünig et al., 2018). These stress-state-dependent processes on the micro-level have also been detected in the experiments with the investigated anisotropic aluminum alloy discussed by Brünig et al. (2021, 2022) where additional dependence on the loading direction with respect to the rolling direction has been revealed.

Experimental and numerically predicted load-displacement curves of the uniaxial tensile tests are shown in Figure 6(a). Good agreement can be seen in the first loading range and especially the

Table 4. Generalized stress parameters for RD.

Experiment	I_1^H [MPa]	$\sqrt{J_2^H}$ [MPa]	J_3^H [MPa^3]	η^H [−]	L^H [−]
Tensile test	1.10E+03	5.57E+02	4.82E+07	3.80E−01	−7.26E−01
Shear test	2.60E+02	5.28E+02	1.05E+07	9.48E−02	−1.86E−01
H 0/1	1.48E+03	4.56E+02	9.60E+06	6.26E−01	−2.62E−01
H 1/0	8.86E+01	5.21E+02	4.35E+06	3.27E−02	−8.02E−02
H 1/0.5	5.21E+02	5.41E+02	2.11E+07	1.85E−01	−3.46E−01
H 1/1	8.90E+02	5.51E+02	3.61E+07	3.11E−01	−5.61E−01
H 1/−1	−5.79E+02	5.23E+02	−2.16E+07	−2.13E−01	3.93E−01
H 1/−2	−1.00E+03	5.47E+02	−3.73E+07	−3.52E−01	5.93E−01
X0 1/0	7.25E+02	4.81E+02	2.65E+07	2.90E−01	−6.19E−01
X0 1/1	1.13E+03	5.14E+02	6.40E+06	4.22E−01	−1.21E−01
X0 1/−1	3.32E+02	4.93E+02	5.77E+06	1.30E−01	−1.26E−01

Table 5. Generalized stress parameters for DD.

Experiment	I_1^H [MPa]	$\sqrt{J_2^H}$ [MPa]	J_3^H [MPa^3]	η^H [−]	L^H [−]
Tensile test	7.55E+02	5.38E+02	5.05E+07	2.70E−01	−8.43E−01
Shear test	6.67E+02	5.88E+02	2.05E+07	2.18E−01	−2.63E−01
H 0/1	1.32E+03	4.66E+02	8.60E+06	5.45E−01	−2.19E−01
H 1/0	3.76E+02	5.23E+02	6.34E+06	1.38E−01	−1.15E−01
H 1/0.5	6.98E+02	5.61E+02	2.70E+07	2.40E−01	−3.97E−01
H 1/1	9.56E+02	5.75E+02	4.33E+07	3.20E−01	−5.92E−01
H 1/−1	−1.43E+02	5.31E+02	−1.87E+07	−5.20E−02	3.25E−01
H 1/−2	−5.32E+02	5.37E+02	−3.31E+07	−1.91E−01	5.56E−01
X0 1/0	4.14E+02	4.83E+02	2.42E+07	1.65E−01	−5.59E−01
X0 1/1	1.27E+03	5.00E+02	7.26E+06	4.87E−01	−1.50E−01
X0 1/−1	3.45E+01	4.82E+02	2.59E+06	1.37E−02	−6.08E−02

direction-dependent load levels are well simulated. Highest loads appear for loading in RD whereas smaller ones can be observed for loading in DD and the differences are about 7%. Discrepancies in the slopes of experimental and numerical curves are taken to be an indicator of onset of damage and are marked by the black points in Figure 6(a). At these points the stress state is analyzed in detail in critical regions of the specimens. In addition, results of the shear tests are shown in Figure 6(b). At the beginning, the experimental curves are close together and the results after further loading might be affected by inhomogeneities in the geometry and the material in the notched parts. This could also be the reason for different loading-direction-dependent trends in the experiments and the numerical simulations. Nevertheless, onset of damage is again assumed to occur when the slopes of the load-displacement curves deviate which is shown by the black points in Figure 6(b) where the stress state is analyzed.

Experimental and numerically predicted load-displacement curves of the biaxially loaded X0-specimen are shown in Figure 7 where results for the different load ratios (a) $F_1/F_2 = 1/0$, (b) $F_1/F_2 = 1/1$, (c) $F_1/F_2 = 1/-1$ can be seen. It should be noted that in Figure 7(c) the negative forces F_2 and the corresponding negative displacements Δu_{ref} are also plotted in the first quadrant of the diagram to allow comparison of tensile and compressive load paths. In all tests good agreement of experimental and numerical curves is obtained and the black points characterizing onset of

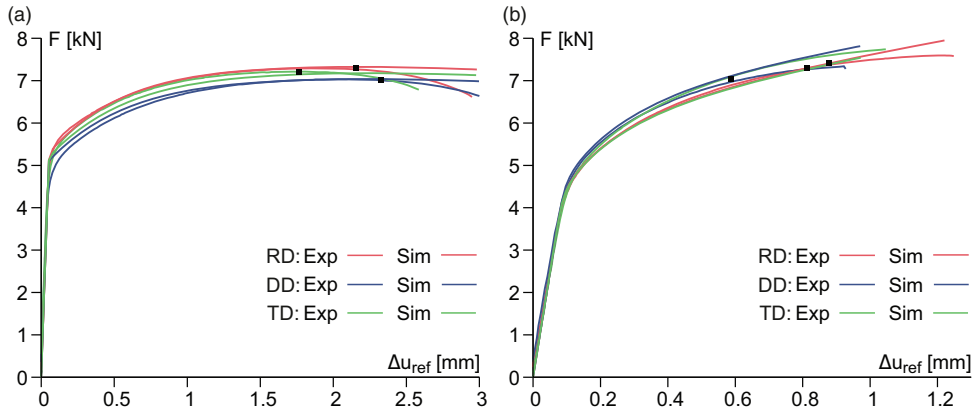

Figure 6. Load-displacement curves of (a) uniaxial tensile tests and (b) shear tests based on experiments (Exp) and numerical simulations (Sim).

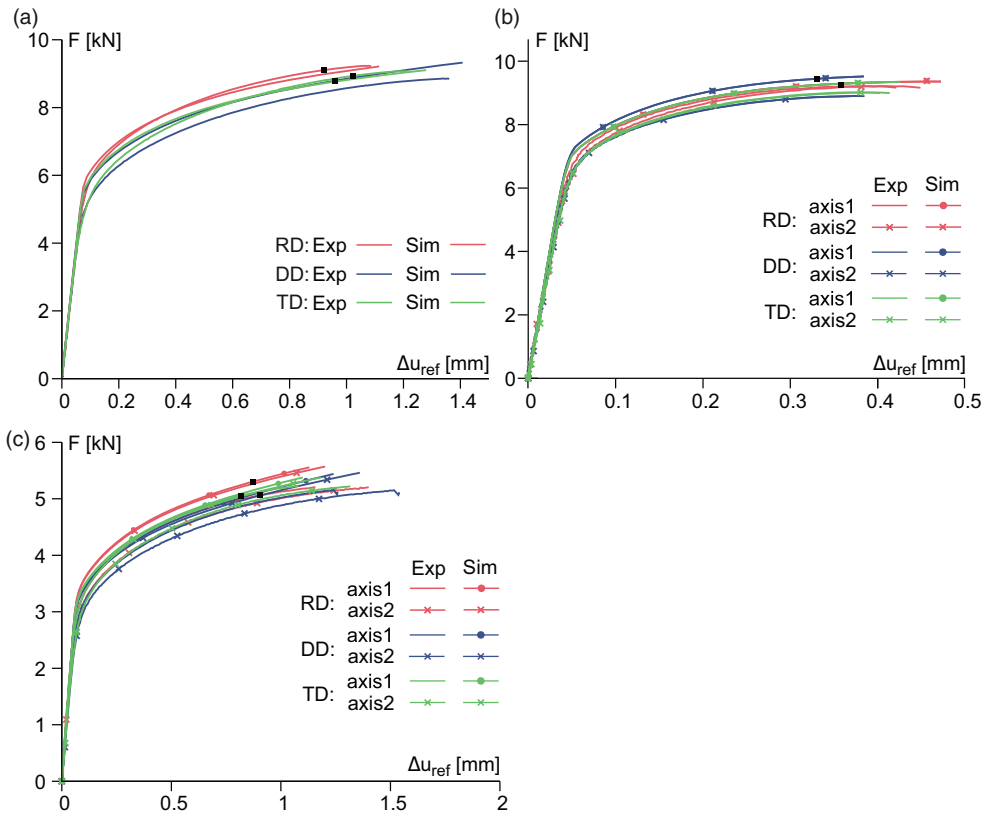

Figure 7. Load-displacement curves for the X0-specimen with (a) $F_1/F_2 = 1/0$, (b) $F_1/F_2 = 1/1$ and (c) $F_1/F_2 = 1/-1$ based on experiments (Exp) and numerical simulations (Sim).

damage are also shown. At these loading stages the stress states in critical parts of the specimens are analyzed in detail and relevant stress parameters are determined.

In addition, experimental and numerically predicted load-displacement curves of the biaxially loaded H-specimen are shown in Figure 8 where results for the different load ratios (a) $F_1/F_2 = 0/1$, (b) $F_1/F_2 = 1/0$, (c) $F_1/F_2 = 1/0.5$, (d) $F_1/F_2 = 1/1$, (e) $F_1/F_2 = 1/-1$, (f) $F_1/F_2 = 1/-2$ can be seen. It should be noted that in Figure 8(e) and (f) the negative forces F_2 and the corresponding

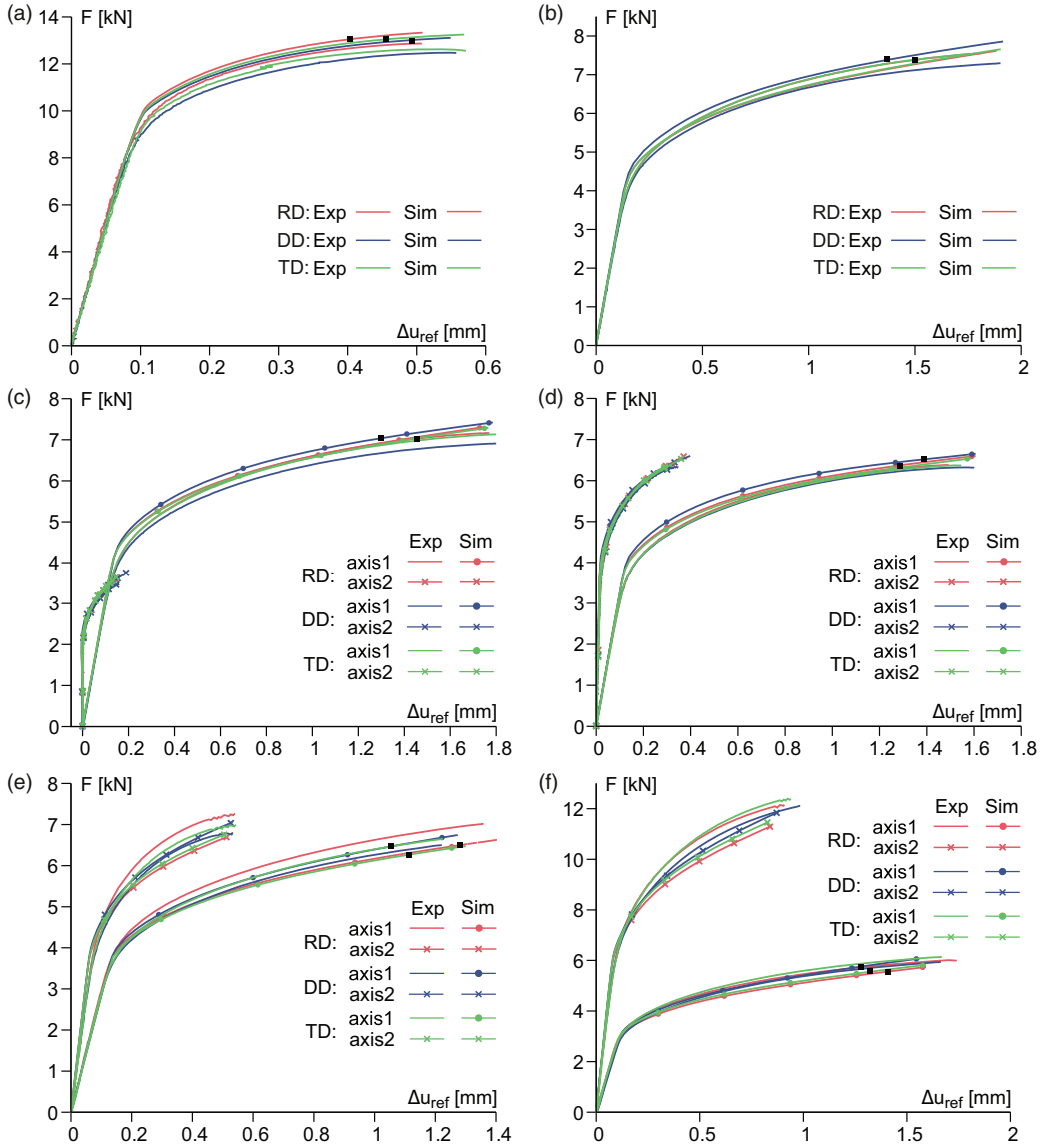

Figure 8. Load-displacement curves for the H-specimen with (a) $F_1/F_2 = 0/1$, (b) $F_1/F_2 = 1/0$, (c) $F_1/F_2 = 1/0.5$, (d) $F_1/F_2 = 1/1$, (e) $F_1/F_2 = 1/-1$ and (f) $F_1/F_2 = 1/-2$ based on experiments (Exp) and numerical simulations (Sim).

negative displacements $\Delta u_{ref.2}$ are also plotted in the first quadrant to allow better comparison of tensile and compressive load paths. In all tests good agreement of experimental and numerical curves is obtained and the black points characterizing onset of damage are also shown. Relevant stress parameters are computed at these stages of the loading path in critical regions of the H-specimens.

Based on the results of the numerical simulations of the experiments with uniaxially and biaxially loaded specimens there are sufficient data (see Tables 4 to 6) enabling development of a quantitative representation of the damage parameters α and β appearing in the damage criterion (17) formulated in the stress and loading direction space, respectively. In particular, in the region of negative stress triaxialities damage is mainly caused by formation and growth of micro-shear-cracks which can be seen as a result of predominant shear stresses. Thus, here the parameters are chosen to be $\alpha = 0$ and $\beta = 1$ leading with the data shown in Tables 4 to 6 to the equivalent damage stress $\sigma = 540$ MPa. In the present investigation the parameter α is chosen to be that one for isotropic plastic behavior based on numerical simulations on the micro-scale (Brünig et al., 2013) valid for all loading directions:

$$\alpha(\eta^H) = \begin{cases} 0 & \text{for } \eta^H \leq 0 \\ \dfrac{1}{3} & \text{for } \eta^H > 0 \end{cases} \tag{31}$$

Analyzing the stress parameters of all experiments with specimens loaded in RD leads to

$$\beta(\eta^H) = \begin{cases} 1 & \text{for } \eta^H \leq 0 \\ 1 - 1.697\,\eta^H & \text{for } \eta^H > 0 \end{cases} \tag{32}$$

showing good agreement with the data points plotted in Figure 9(b). In addition, based on the tests with specimens loaded in DD the function

$$\beta(\eta^H) = \begin{cases} 1 & \text{for } \eta^H \leq 0 \\ 1 - 1.595\,\eta^H & \text{for } \eta^H > 0 \end{cases} \tag{33}$$

Table 6. Generalized stress parameters for TD.

Experiment	I_1^H [MPa]	$\sqrt{J_2^H}$ [MPa]	J_3^H [MPa^3]	η^H [−]	L^H [−]
Tensile test	4.58E+02	5.00E+02	3.14E+07	1.76E−01	−6.53E−01
Shear test	1.38E+02	5.18E+02	8.80E+06	5.13E−02	−1.64E−01
H 0/1	1.13E+03	4.53E+02	7.78E+06	4.82E−01	−2.16E−01
H 1/0	1.14E+01	5.22E+02	3.31E+06	4.21E−03	−6.07E−02
H 1/0.5	2.55E+02	5.42E+02	1.84E+07	9.08E−02	−3.01E−01
H 1/1	4.61E+02	5.16E+02	2.53E+07	1.72E−01	−4.79E−01
H 1/−1	−4.32E+02	5.27E+02	−2.03E+07	−1.58E−01	3.62E−01
H 1/−2	−7.53E+02	5.47E+02	−3.50E+07	−2.65E−01	5.55E−01
X0 1/0	2.24E+02	4.74E+02	2.22E+07	9.11E−02	−5.44E−01
X0 1/1	1.11E+03	5.01E+02	6.35E+06	4.25E−01	−1.29E−01
X0 1/−1	2.70E+02	4.68E+02	1.04E+06	1.11E−01	2.60E−02

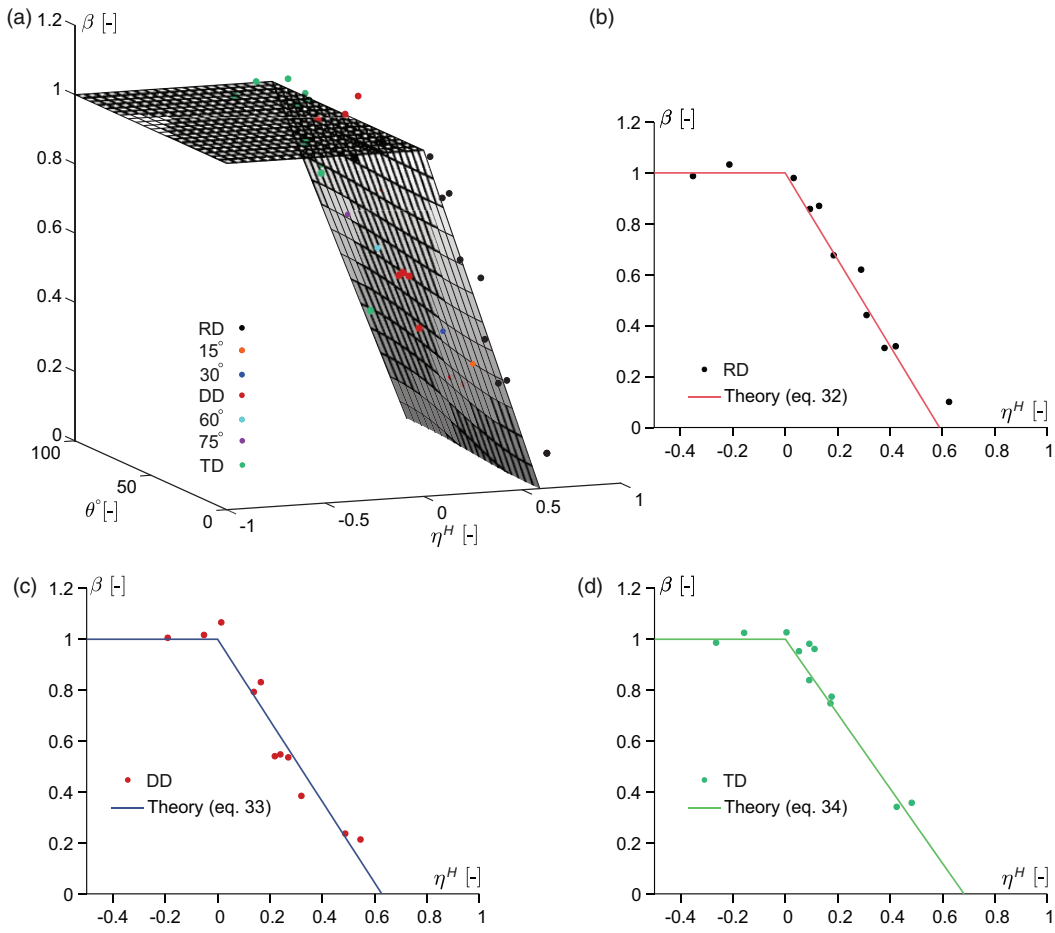

Figure 9. Parameter β depending on the generalized stress triaxiality η^H and the loading direction θ.

is developed, and good agreement of data points and this curve can be seen in Figure 9(c). In the same way, the results of the experiments with specimens loaded in TD are used to propose

$$\beta(\eta^H) = \begin{cases} 1 & \text{for } \eta^H \leq 0 \\ 1 - 1.467\,\eta^H & \text{for } \eta^H > 0 \end{cases} \tag{34}$$

also showing good agreement with the data points, see Figure 9(d). It should be noted that based on the available data a clear dependence of the parameter β on the generalized stress triaxiality η^H can be detected whereas it is difficult to reveal an additional influence of the generalized Lode parameter L^H. Thus, possible effect of the Lode parameter L^H is not considered in the present paper examining experimental results and will be studied in future work dealing with numerical simulations on the micro-scale for the investigated anisotropic aluminum alloy.

However, different parameters β have been developed for loading of the specimens in RD, DD and TD and, thus, dependence on the angle of loading direction θ is evident. Using equations (32) to (34) the multiplicative dependence for the function

$$\beta(\eta^H, \theta) = \begin{cases} 1 & \text{for } \eta^H \leq 0 \\ k(\theta)\,\eta^H + 1 & \text{for } \eta^H > 0 \end{cases} \tag{35}$$

is proposed with the loading-direction-dependent factor

$$k(\theta) = -0.167\cos^2\theta - 0.062\cos\theta - 1.467 \tag{36}$$

If, based on equation (35) a negative value is computed, β is taken to be zero. This is the case for high positive stress states where damage is mainly caused by growth of voids which is an effect of high hydrostatic tensile stress (high I_1^H) and, then, the influence of J_2^H is marginal. The dependence of the damage parameter β on both the generalized stress triaxiality η^H and the angle of loading direction θ is visualized in Figure 9(a) showing good agreement with available data points. In this diagram also results of further uniaxially loaded tensile specimens are added for $\theta = 15^\circ, 30^\circ, 60^\circ$, and 75° which had been used to examine plastic anisotropy (see Brünig et al., 2021). In summary, the results have clearly shown that plastic anisotropy affects the damage behavior of the investigated aluminum alloy.

Conclusions

In the present paper a damage criterion for ductile metals with plastic anisotropy has been proposed. A series of experiments with uniaxially loaded tension/compression and shear specimens as well as with the biaxially loaded X0- and H-specimens deliver data for identification of stress-state- and loading-direction-dependent damage mode functions. Anisotropic plastic behavior of the investigated aluminum alloy EN AW-2017A is modeled by the Hoffman yield condition taking into account the strength-differential effect which has been observed in the tension and compression tests. Evolution of isochoric plastic strains is based on Hill's plastic potential function leading to a non-associated flow rule. Based on the Hoffman criterion generalized anisotropic stress invariants as well as the generalized stress triaxiality and the generalized Lode parameter have been defined. The damage condition for anisotropic ductile metals has been formulated in terms of the generalized stress invariants. Damage mode parameters are used to combine the anisotropic stress variables in an adequate manner taking into account in a phenomenological way the different damage and failure mechanisms acting on the micro-scale. The functions of the damage mode parameters depend on both the stress state and the loading direction with respect to the rolling direction. The proposed damage model can be seen as an efficient framework to numerically simulate the anisotropic behavior of materials in various engineering applications.

Declaration of conflicting interests

The author(s) declared no potential conflicts of interest with respect to the research, authorship, and/or publication of this article.

Funding

The author(s) disclosed receipt of the following financial support for the research, authorship, and/or publication of this article: The authors received financial support from the Deutsche Forschungsgemeinschaft (DFG, German Research Foundation) under project number 394286626 (BR1793/20-1).

ORCID iD


Michael Brünig https://orcid.org/0000-0002-6338-4238

References

Abu Al-Rub RK and Voyiadjis G (2003) On the coupling of anisotropic damage and plasticity models for ductile materials. *International Journal of Solids and Structures* 40: 2611–2643.

Badreddine H and Saanouni K (2017) On the full coupling of plastic anisotropy and anisotropic ductile damage under finite strain. *International Journal of Damage Mechanics* 26: 1080–1123.

Badreddine H, Saanouni K and Nguyen TD (2015) Damage anisotropy and its effect on the plastic anisotropy evolution under finite strains. *International Journal of Solids and Structures* 63: 11–31.

Bai Y and Wierzbicki T (2008) A new model of metal plasticity and fracture with pressure and lode dependence. *International Journal of Plasticity* 24: 1071–1096.

Barlat F, Aretz H, Yoon JW, et al. (2005) Linear transformation-based anisotropic yield functions. *International Journal of Plasticity* 21: 1009–1039.

Barlat F, Lege DJ and Brem JC (1991) A six-component yield function for anisotropic materials. *International Journal of Plasticity* 7: 693–712.

Bao Y and Wierzbicki T (2004) On the fracture locus in the equivalent strain and stress triaxiality space. *International Journal of Mechanical Sciences* 46: 81–98.

Bonora N, Gentile D, Pirondi A, et al. (2005) Ductile damage evolution under triaxial state of stress: Theory and experiments. *International Journal of Plasticity* 21: 981–1007.

Brünig M (1999) Large strain elastic-plastic theory and nonlinear finite element analysis based on metric transformation tensors. *Computational Mechanics* 24: 187–196.

Brünig M (2003) An anisotropic ductile damage model based on irreversible thermodynamics. *International Journal of Plasticity* 19: 1679–1713.

Brünig M (2016) A thermodynamically consistent continuum damage model taking into account the ideas of CL chow. *International Journal of Damage Mechanics* 25: 1130–1143.

Brünig M, Brenner D and Gerke S (2015a) Modeling of stress-state-dependent damage and failure of ductile metals. *Applied Mechanics Materials* 784: 35–42.

Brünig M, Brenner D and Gerke S (2015b) Stress state dependence of ductile damage and fracture behavior: Experiments and numerical simulations. *Engineering Fracture Mechanics* 141: 152–169.

Brünig M, Chyra O, Albrecht D, et al. (2008) A ductile damage criterion at various stress triaxialities. *International Journal of Plasticity* 24: 1731–1755.

Brünig M, Gerke S and Hagenbrock V (2013) Micro-mechanical studies on the effect of the stress triaxiality and the lode parameter on ductile damage. *International Journal of Plasticity* 50: 49–65.

Brünig M, Gerke S and Koirala S (2021) Biaxial experiments and numerical analysis on stress-state-dependent damage and failure behavior of the anisotropic aluminum alloy EN AW-2017A. *Metals* 11: 1214.

Brünig M, Gerke S and Schmidt M (2018) Damage and failure at negative stress triaxialities. *International Journal of Plasticity* 102: 70–82.

Brünig M, Gerke S and Zistl M (2019) Experiments and numerical simulations with the H-specimen on damage and fracture of ductile metals under non-proportional loading paths. *Engineering Fracture Mechanics* 217: 106531.

Brünig M, Koirala S and Gerke S (2022) Analysis of damage and failure in anisotropic ductile metals based on biaxial experiments with the H-specimen. *Experimental Mechanics* 62: 183–197.

Chaboche J-L (1988) Continuum damage mechanics. Part I: General concepts. *Journal of Applied Mechanics* 55: 59–64.

Chow C and Wang J (1987) An anisotropic theory of continuum damage mechanics for ductile fracture. *Engineering Fracture Mechanics* 27: 547–558.
Demmerle S and Boehler J (1993) Optimal design of biaxial tensile cruciform specimens. *Journal of the Mechanics and Physics of Solids* 41: 143–181.
Driemeier L, Brünig M, Micheli G, et al. (2010) Experiments on stress-triaxiality dependence of material behavior of aluminum alloys. *Mechanics of Materials* 42: 207–217.
Dunand M and Mohr D (2011) On the predictive capabilities of the shear modified Gurson and the modified Mohr-Coulomb fracture models over a wide range of stress triaxialities and lode angles. *Journal of the Mechanics and Physics of Solids* 59: 1374–1394.
Gao X, Zhang G and Roe C (2010) A study on the effect of the stress state on ductile fracture. *International Journal of Damage Mechanics* 19: 75–94.
Gerke S, Adulyasak P and Brünig M (2017) New biaxially loaded specimens for analysis of damage and fracture in sheet metals. *International Journal of Solids and Structures* 110: 209–218.
Gerke S, Zistl M and Brünig M (2020) Experiments and numerical simulation of damage and fracture of the X0-specimen under non-proportional loading paths. *Engineering Fracture Mechanics* 224: 106795.
Green D, Neale K, MacEwen S, et al. (2004) Experimental investigation of the biaxial behaviour of an aluminum sheet. *International Journal of Plasticity* 20: 1677–1706.
Ha J, Baral M and Korkolis Y (2018) Plastic anisotropy and ductile fracture of bake-hardened AA6013 aluminum sheet. *International Journal of Solids and Structures* 155: 123–139.
Hill R (1948) A theory of the yielding and plastic flow of anisotropic metals. *Proceedings of the Royal Society London* 193: 281–297.
Hoffman O (1967) The brittle strength of orthotropic materials. *Journal of Composite Materials* 1: 200–206.
Hosseini N, Nieto-Fuentes JC, Dakshinamurthy M, et al. (2022) The effect of material orientation on void growth. *International Journal of Plasticity* 148: 103149.
Hu Q, Yoon JW, Manopulo N, et al. (2021) A coupled yield criterion for anisotropic hardening with analytical description under associated flow rule: Modeling and validation. *International Journal of Plasticity* 136: 102882.
Kulawinski D, Nagel K, Henkel S, et al. (2011) Characterization of stress-strain behavior of a cast trip steel under different biaxial planar load ratios. *Engineering Fracture Mechanics* 78: 1684–1695.
Kuwabara T (2007) Advances in experiments on metal sheet and tubes in support of constitutive modeling and forming simulations. *International Journal of Plasticity* 23: 385–419.
Lemaitre J (1985) Coupled elasto-plasticity and damage constitutive equations. *Computer Methods in Applied Mechanics and Engineering* 51: 31–49.
Lin S and Ding J (1995) Experimental study of the plastic yielding of rolled sheet metals with the cruciform plate specimen. *International Journal of Plasticity* 11: 583–604.
Li H, Fu MW, Lu J, et al. (2011) Ductile fracture: Experiments and computations. *International Journal of Plasticity* 27: 147–180.
Liu Y, Kang L and Ge H (2019) Experimental and numerical study on ductile fracture of structural steels under different stress states. *Journal of Constructional Steel Research* 158: 381–404.
Lou Y and Huh H (2017) Extension of a shear controlled ductile fracture model considering the stress triaxiality and the lode parameter. *International Journal of Solids and Structures* 50: 447–455.
Lou Y, Chen L, Clausmeyer T, et al. (2017) Modeling of ductile fracture from shear to balanced biaxial tension for sheet metals. *International Journal of Solids and Structures* 112: 169–184.
Lou Y, Huh H, Lim S, et al. (2012) New ductile fracture criterion for prediction of fracture forming limit diagrams of sheet metals. *International Journal of Solids and Structures* 49: 3605–3615.
Müller W and Pöhland K (1996) New experiments for determining yield loci of sheet metal. *Material Processing Technology* 60: 643–648.
Park N, Huh H and Yoon JW (2018) Anisotropic fracture forming limit diagram considering non-directionality of the equi-biaxial fracture strain. *International Journal of Solids and Structures* 151: 181–194.
Park N, Huh H, Lim SJ, et al. (2017) Fracture-based forming limit criteria for anisotropic materials in sheet metal forming. *International Journal of Plasticity* 96: 1–35.

Roth C and Mohr D (2016) Ductile fracture experiments with local proportional loading histories. *International Journal of Plasticity* 79: 328–354.

Scales M, Chen K and Kyriakides S (2019) Material response, localization, and failure of an aluminum alloy under combined shear and tension: Part I experiments. *International Journal of Plasticity* 120: 340–360.

Song X, Leotoing L, Guines D, et al. (2017) Characterization of forming limits at fracture with an optimized cruciform specimen: Application to DP600 steel sheets. *International Journal of Mechanical Sciences* 126: 35–43.

Spitzig WA and Richmond O (1984) The effect of pressure on the flow stress of metals. *Acta Metallurgica* 32: 457–463.

Spitzig WA, Sober RJ and Richmond O (1975) Pressure dependence of yielding and associated volume expansion in tempered martensite. *Acta Metallurgica* 23: 885–893.

Spitzig WA, Sober RJ and Richmond O (1976) The effect of hydrostatic pressure on the deformation behavior of maraging and HY-80 steels and its implications for plasticity theory. *Metallurgical Transactions* 7A: 1703–1710.

Stoughton TB and Yoon JW (2009) Anisotropic hardening and non-associated flow rule in proportional loading of sheet metals. *International Journal of Plasticity* 25: 1777–1817.

Tsutamori H, Amaishi T, Chorman RR, et al. (2020) Evaluation of prediction accuracy for anisotropic yield functions using cruciform hole expansion test. *Journal of Manufacturing and Materials Processing* 4: 43.

Wei Z, Zistl M, Gerke S, et al. (2022) Analysis of ductile damage and fracture under reverse loading. *International Journal of Mechanical Sciences* 228: 107476.